DOI: 10.13009/EUCASS2019-176

Modelling and Simulation of Very Low Earth Orbits

D. González[1†], V. Cañas[1†], J. Becedas[1], R. M. Domínguez[1], P. C. E. Roberts[2], N. H. Crisp[2], V. T. A. Oiko[2], S. Edmondson[2], S. D. Worrall[2], S. Haigh[2], K. Smith[2], R. E. Lyons[2], S. Livadiotti[2], C. Huyton[2], L. A. Sinpetru[2], S. Rodriguez-Donaire[3], D. Garcia-Almiñana[3], M. Nieto[3], C. Muñoz[3], M. Sureda[3], D. Kataria[4], G. H. Herdrich[5], F. Romano[5], T. Binder[5], A. Boxberger[5], S. Fasoulas[5], C. Traub[5], R. Outlaw[6], L. Ghizoni[7], V. Jungnell[7], K. Bay[7], J. Morsbøl[7], R. Villain[8], J. S. Perez[8], A. Conte[8], B. Belkouchi[8], A. Schwalber[9], B. Heißerer[9]

[1]Elecnor Deimos Satellite Systems, Calle Francia 9, 13500 Puertollano, Spain

david.gonzalez@deimos-space.com, valentin-jose.canas@deimos-space.com

[2]The University of Manchester, Oxford Road, Manchester, M13 9PL – United Kingdom.

[3]UPC-Barcelona TECH, Carrer de Colom 11, 08222 Terrassa, Barcelona, Spain.

[4]Mullard Space Science Laboratory (UCL), Holmbury St. Mary, Dorking, RH5 6NT, United Kingdom.

[5]Institute of Space System, University of Stuttgart, Pfaffenwaldring 29, 70569 Stuttgart, Germany.

[6]Christopher Newport University, 1 Avenue of the Arts, Newport News, VA 23606, USA.

[7]Gomspace AS, Langagervej 6, 9220 Aalborg East, Denmark.

[8]Euroconsult, 86 Boulevard de Sébastopol, 75003 Paris, France.

[9]Concentris Research Management GmbH, Ludwigstraße 4, D-82256 Fürstenfeldbruck, Germany

† These authors equally contributed to the paper.

Abstract

Flying a satellite at very low earth orbit is a technological challenge. It presents advantages, such as increase resolution in optical payloads, reduce costs of launch and enhance the use of air breathing propulsion and specular materials. The density of the atmosphere at these altitudes is much higher, behaving as a free molecular flow. This has severe implications in the increase of drag torques and forces that has to be analyzed in depth. We analyze the effects and the perturbations to small satellites, affecting their dynamics, performance and lifetime by implementing and analyzing realistic models of the environment at VLEO.

1. Introduction

In the last years the interest in VLEO has increased because of the advantages of orbits in altitudes lower than 450 km [1]: flying at these altitudes increases the signal to noise ratio for the communications, revisit time can be increased, optical payloads can provide higher resolution imagery, VLEO orbits have less population of space debris and have less propagation delay than higher orbits, among others. However, VLEO missions must face challenges due to the change in the atmosphere density and its composition it can drastically reduce the lifetime (because of gas-surface interactions with free molecular flow) and increase corrosion (produced by atomic oxygen). Gas-surface interactions increase the drag forces and torques affecting a satellite flying at these low altitudes and, for instance, their operations can be significantly different compared with satellites flying at higher altitudes.

The effects of drag and lift on a spacecraft have been extensively reviewed in the literature. The interaction between the atmosphere particles and the surfaces of the spacecraft is responsible for the aerodynamic torques and forces. In VLEO, due to the low density, the atmospheric fluid behaviour has to be considered a free molecular flow and it has important implications when modelling the system [5]. Several models have been proposed to model gas surface interactions (GSI) in this rarefied environment [6] and [7]. One of the most used GSI models was proposed by Sentman [7]. Several analytical solutions have been tested to do the analysis of GSI models in the literature: Direct Simulation Monte Carlo (DSMC) [8], analytical methods based on panels [9] and [10] or Test Particle Monte Carlo (TPMC) [14]. DSMC simulates molecules collisions, which accurately model the interaction between atmospheric particles and the satellite surface, but it requires large computation resources and time. The panel methods have the advantage of requiring less computing resources, what makes it very agile to be implemented for online or real time

DOI: 10.13009/EUCASS2019-176

computations. However, panel methods have an important limitation when analysing concave surfaces, because they do not usually consider multiple reflections and collisions of particles.

The impact of the space environment at VLEO in the lifetime of a satellite was previously analysed by Pulido [11]. More recent research has focused on the analysis of the different methods and their application in different scenarios to get results [12], [13] and [14], its application in attitude control simulations [15] or the use of drag and lift for manoeuvres [16].

In this paper we present the characteristics of the VLEO environment and how it affects to the performance of a satellite. Results comparing a satellite flying at LEO and at VLEO are shown, and the main differences are highlighted. This work is part of the H2020 DISCOVERER project. Project ID 737183.

2. Materials and methods

2.1 Environmental models and perturbations

Environment perturbation torques acting on a satellite in orbit include gravity gradient, solar radiation, aerodynamic torque and Earth's magnetic field. The gravity gradient is the spatial rate of change of gravitational acceleration and it is produced around the centre of mass of the satellite. Solar radiation perturbation is caused by the force created by the transfer of momentum of the absorbed photons to the spacecraft. The aerodynamic torque is originated by the interaction between the surfaces of the satellite and the upper atmosphere particles. It is considered as the main perturbation in VLEO satellites. Finally, the Earth's magnetic field has influence in the motion of a satellite too. The currents in the satellite generate a magnetic dipole that creates a torque in presence of the Earth's magnetic field.

In order to get realistic values of the perturbations affecting the satellite the following models were used:

- Atmospheric model: The Drag Temperature Model DTM2013 [3]
- Earth's magnetic field model: International Geomagnetic Reference Field IGRF12 [2]
- Atmospheric wind: Horizontal Wind Model HWM14 [4].

The Drag Temperature Model (DTM2013) is a semi-empirical model which provides the temperature, density, and composition of the Earth's thermosphere. It is tuned with data provided by CHAMP, GRACE and GOCE spacecrafts. This model covers the 200–900 km altitude range and includes information from solar activity. DTM2013 was developed by including data from the DTM2009 model, but incorporates more data from GRACE and GOCE in particular.

The 12th generation of the International Geomagnetic Reference Field (IGRF12) updates the previous IGRF generation with an ultimate main field model for epoch 2010.0, a main field model for epoch 2015.0, and a linear annual predictive secular variation model for 2015.0-2020.0. Figure 1 shows the magnetic field calculated with IGRF12 model at an altitude of 300 km.

HWM14 is an update to the HWM07 empirical model for horizontal winds in the troposphere, stratosphere, mesosphere, and thermosphere. In the thermosphere, the model consists of two parts: a quiet-time part (without geomagnetic influence) and a geomagnetically disturbed part. It does not consider solar activity dependence.

DOI: 10.13009/EUCASS2019-176

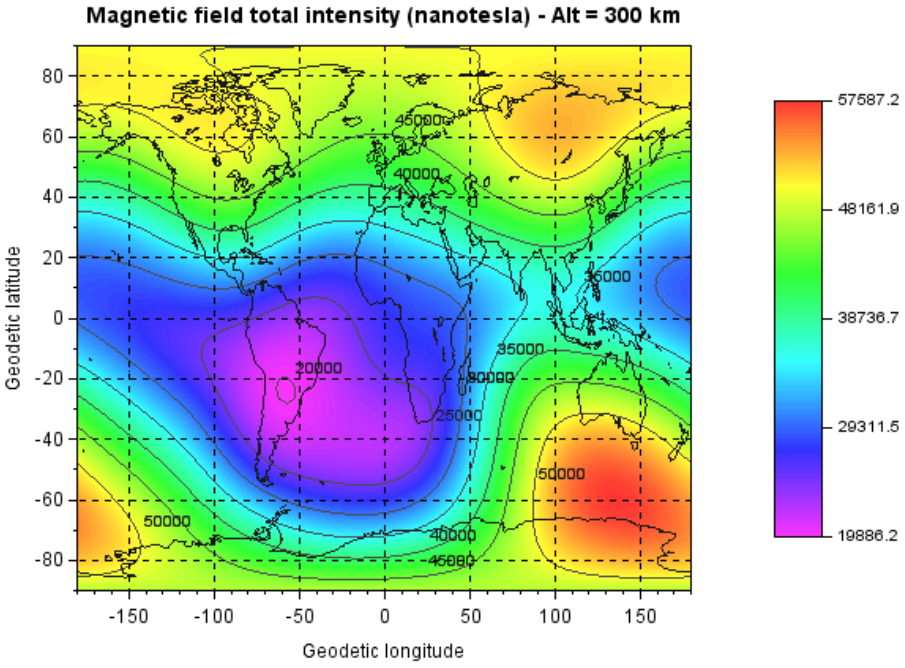

Figure 1: Magnetic field at 300 km

The analysis of the perturbations with models that are more accurate facilitate the estimation of more realistic environmental perturbations. The perturbations were computed as follows:

- Magnetic torque $\vec{T}_{mag_q}$ (*Nm*):

$$\vec{T}_{mag_q} = \vec{m}_q \times \vec{B}_q \quad \textbf{(1)}$$

where, $\vec{m}_q$ (Nm/T)is the magnetic dipole of the satellite and $\vec{B}_q$(T) is the magnetic field of the Earth.

- Gravity gradient torque $\vec{T}_{gravity}$ (*Nm*), where μ is the gravitational constant of the Earth, which can be calculated as $\mu=GM$, with G the universal gravitational constant (6.674×10^{-11} Nm^2/kg^2) and *M* the mass of the Earth (5972×10^{24} *kg*) being; R is the distance from the centre of the Earth to the orbit of the satellite.

$$\vec{T}_{gravity} = \frac{3\mu}{R^2}\begin{bmatrix}(I_{zz}-I_{yy})b_1c_1\\(I_{xx}-I_{zz})a_1c_1\\(I_{xx}-I_{zz})a_1c_1\end{bmatrix} \quad \textbf{(2)}$$

where μ is the gravitational constant of the Earth, which can be calculated as $\mu=GM$, with G the universal gravitational constant (*6.674 x 10-11 Nm2/kg2*) and M the mass of the Earth (*5972 x 1024 kg*); R is the distance from the centre of the Earth to the orbit of the satellite; Ixx, Iyy and Izz the diagonal elements of the inertia matrix (kg/m^4) and a_1, b_1 and c_1 coeficients defined as follows in quaternions notation:

$$\begin{aligned} a_1 &= 2q_1q_3 - 2q_2q_4 \\ b_1 &= 2q_2q_3 + 2q_1q_4 \\ c_1 &= 2q_4^2 + 2q_3^2 - 1 \end{aligned} \quad \textbf{(3)}$$

- Aerodynamic torque $\vec{T}_{aero}$ *(Nm)*:

$$\vec{T}_{aero} = \sum_{i=1}^{n} (\vec{F}_{D_i} \times \vec{F}_{L_i}) \times \vec{r}_i \quad \textbf{(4)}$$

DOI: 10.13009/EUCASS2019-176

Being $\vec{r}_i$ the position vector between the geometric centre of the satellite and the centre of pressure of the panel and $\vec{F}_{L_i}$ and $\vec{F}_{D_i}$ lift force and the drag force for each panel respectively and the aerodynamic force $\vec{F}_{aero}$ (N) as follows:

$$\vec{F}_{aero} = \sum_{i=1}^{n} (\vec{F}_{D_i} \times \vec{F}_{L_i}) \tag{5}$$

Where $\vec{F}_{L_i}$ (N) and $\vec{F}_{D_i}$ (N) are defined as:

$$F_{D_i} = \frac{1}{2} \rho C_d \vec{V}_{aero}^2 A_i \tag{6}$$

$$F_{L_i} = \frac{1}{2} \rho C_l \vec{V}_{aero}^2 A_i \tag{7}$$

Being C_l the lift coefficient, C_d the drag coefficient, A_i the panel surface (m^2), ρ the density (kg/m^3) and $\vec{V}_{aero}$ the aerodynamic velocity (m/s):

$$\vec{V}_{aero} = \vec{V}_{orb} + \vec{V}_{wind} \tag{8}$$

Where $\vec{V}_{orb}$ is the orbital velocity (m/s) and $\vec{V}_{wind}$ the wind velocity (m/s).

2.2 Simulation environment

The tool used to run the simulations was Scilab (version 6.0.1) with its graphical modelling tool, Xcos. Scilab is a software tool for numerical computation. It implements a collection of numerical algorithms covering several fields of knowledge, such as aeronautics, thermal and fluid dynamics, signal and image processing, among others. It can be used to solve many aspects of scientific computing problems. Xcos is an open source graphical tool to design models using functional blocks. It provides a palette of basic blocks that can be used to solve differential equations and facilitate object oriented computation. It also facilitates the creation of functional blocks with source code in C, C++ or Fortran. This functionality was used to extend the palette of blocks available in the tool and add all the elements required for simulating VLEO environmental conditions and compute all the disturbances affecting the satellite.

As stated before, aerodynamic forces are the main disturbances acting on a spacecraft in VLEO. A panel method implementation was developed and used in this work in order to calculate aerodynamic forces affecting the spacecraft. In this method the spacecraft surface was modelled as a composition of simple panels. The forces and torques produced by GSI where calculated for each panel and after that they were combined to obtain the overall component. The gas-surface interaction was modelled by using Sentman's model equations [7]. The dimensionless drag coefficient C_d can be calculated as follows:

$$C_d = \left\{ \frac{P}{\sqrt{\pi}} + QZcos(\theta) + \frac{\cos(\theta)}{2} \frac{V_{re}}{V_{inc}} (\sqrt{\pi} Zcos(\theta) + P) \right\} \frac{A}{A_{ref}} \tag{9}$$

$$C_l = \left\{ GZsin(\theta) + \frac{\sin(\theta)}{2} \frac{V_{re}}{V_{inc}} (\sqrt{\pi} Zcos(\theta) + P) \right\} \frac{A}{A_{ref}} \tag{10}$$

$$P = \frac{1}{S} e^{-S^2 \cos^2(\theta)} \tag{11}$$

$$G = \frac{1}{2S^2} \tag{12}$$

$$Q = 1 + G \tag{13}$$

$$Z = 1 + \text{erf}\,(Scos(\theta)) \tag{14}$$

DOI: 10.13009/EUCASS2019-176

$$\frac{V_{re}}{V_{inc}} = \sqrt{\frac{1}{2}[1 + \sigma_a(\frac{4RT_W}{V_{inc}^2} - 1)]} \quad \textbf{(15)}$$

where, C_d is the dimensionless drag coefficient and C_l is the dimensionless lift coefficient. θ is the angle (in radians) between the velocity vector and the normal vector to the surface (0 *rads* indicate that the surface is perpendicular to the flux and $\pi/2$ when they are parallel), S is the dimensionless ratio between the orbital velocity, V_∞ (*m/s*), and the most probable random speed of the molecules, *C* (m/s). This is defined as $C_m = \sqrt{2\frac{R}{m}T_i}$, in which *R* is the ideal gas constant (*J/(mol ºK))*, *m* (*kg/mol*) is the mean atomic gas mass of the molecules constituting the atmosphere and T_i (*ºK*) is the temperature of the incident particles. Hence, $\frac{V_\infty}{C_m}$. V_{re} (*m/s*) and V_{inc} (*m/s*) are the velocities of the reflected and the incident molecules, T_w (*ºK*) is the temperatures of the surface wall and *A* (m^2) is the area of the panel surface A_{ref} (m^2) is a reference area, which was defined as follows for the calculations carried out in this paper:
i) for the case of 1U, 1.5U, 2U and 3U CubeSats, the reference area was the area of a face of a 1U CubeSat, or its base, (*10cm x 10cm*), ii) for the case of the 12U, the reference area was *10cm x 20cm* (the base of the CubeSat), and iii) for the 8U, 12U and 16U, the reference area was *20cm x 20cm* (the base of the CubeSats). See Figure 2. Figure 3 shows the 1U geometry considered for the calculations.
For the calculations the values considered for the thermal accommodation coefficient and surface temperature were $\sigma_a = 0.95$ and $T_W = 400K$.

Figure 4 shows the variation of the drag and lift coefficients with variations of θ. The results indicate that the drag coefficient is always higher than the lift coefficient, and that with low values of θ, the drag is several orders of magnitude higher than the lift.

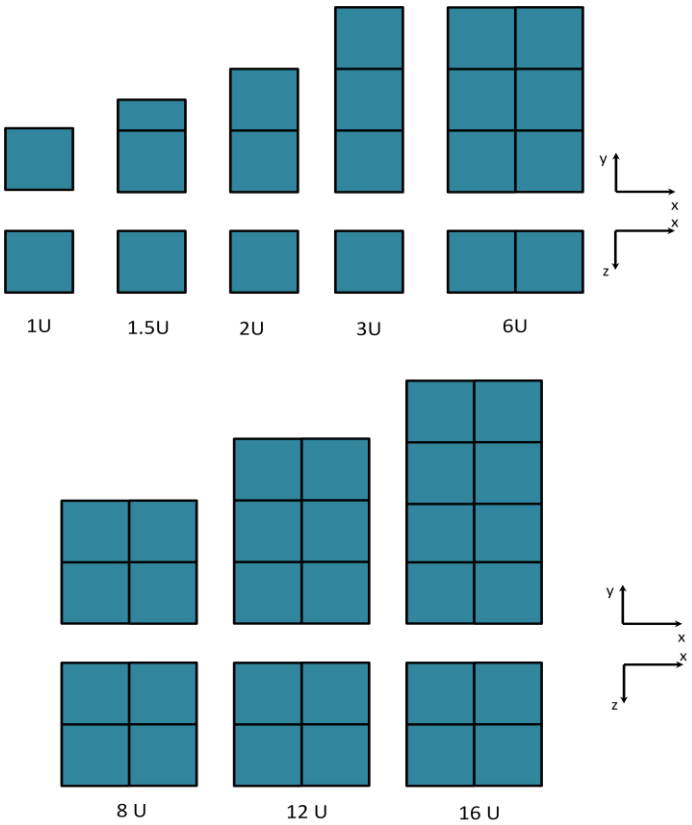

Figure 2: CubeSats sizes used in the calculations

DOI: 10.13009/EUCASS2019-176

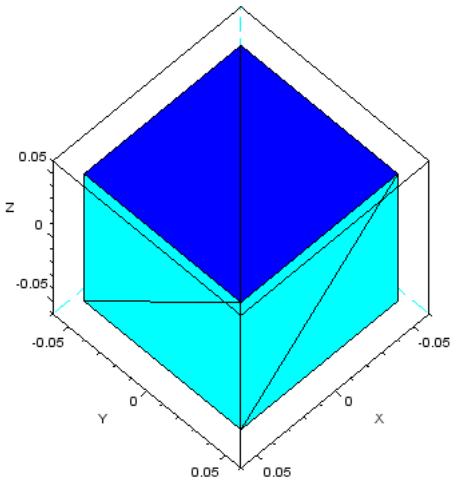

Figure 3: Aproximation of the 1U CubeSat satellite used in the calculations

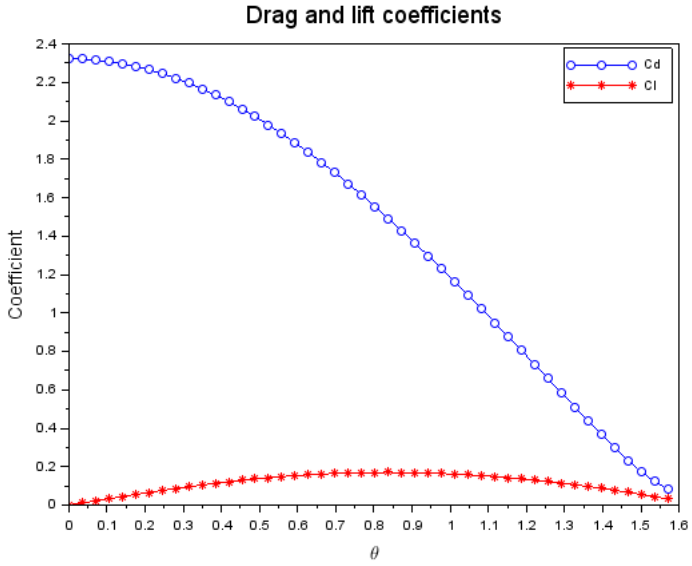

Figure 4: Drag and lift coefficients

In order to establish a comparison between a satellite flying at LEO and VLEO two different cases were considered: 700 km and 350 km orbits. For calculations, the launch date was 3rd April 2012 at 18:00:00. The orbit parameters are defined in Table 1.

Table 1: Orbits used in simulations

	Altitude (km)	**Inclination (degrees)**	**Arg. Perigee (degrees)**	**Mltan (h)**	**Eccentricity**
LEO	700	50	90	12	0.001
VLEO	350	50	90	12	0.001

DOI: 10.13009/EUCASS2019-176

3. Results

3.1 Results

Figure 5a shows the density of the atmosphere at 700km altitude and Figure 5b shows the density of the atmosphere at 350km altitude along the orbits. The value of the density changes in function of the sun radiation in the position of the orbit. In both figures, between 40º and 70º inclinations the density of the atmosphere reached the highest values, more specifically, at 700km the maximum density reached $6.05 \cdot 10^{-14}$ kg/m^3 at -70º of inclination, and the minimum density was $1.28 \cdot 10^{-14}$ kg/m^3 at 128º of inclination; and for VLEO orbit, the maximum density reached the maximum density value of $1.17 \cdot 10^{-11}$ kg/m^3 at a longitude of -63º, while the minimum density was $4.35 \cdot 10^{-11}$ kg/m^3 at 128º longitude. Notice that at VLEO the density of the atmosphere is three orders of magnitude higher that at LEO.

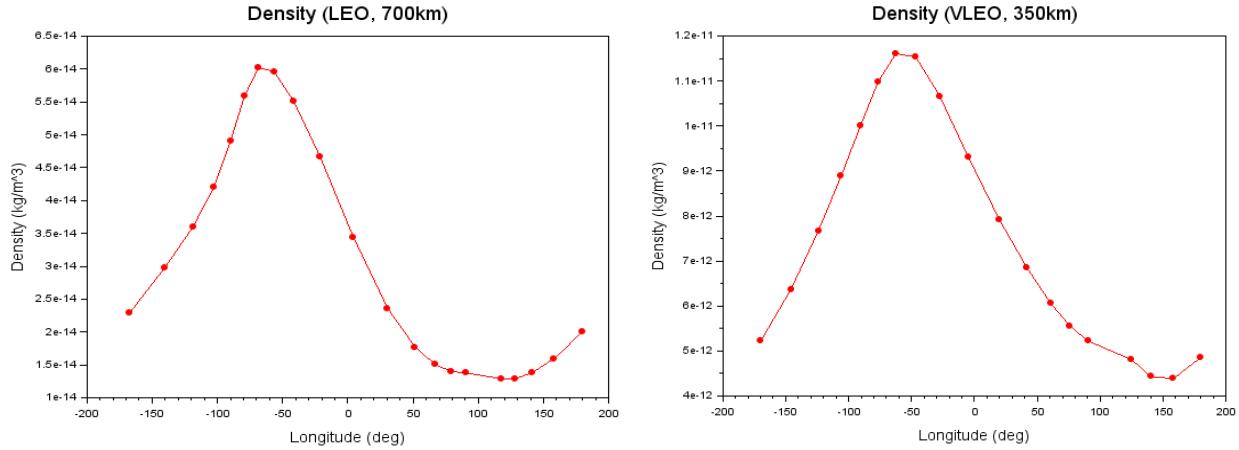

Figure 5: Atmospheric density (a) and atmospheric density (b) in VLEO

Figure 6a depicts the three components of the magnetic field at LEO and VLEO (North, East and Down). Notice that at LEO and at VLEO the components of the magnetic field are quite similar in shape, and in the case of East and Down components are almost coincident. However, in the case of the North component, at VLEO has higher magnitude because it is closer the surface of the Earth.

Figure 6b shows the two horizontal components of atmospheric wind at LEO and VLEO (Meridional and Zonal). It is remarkable that both components are quite similar in shape at LEO and VLEO. Besides, the wind rises at longitudes corresponding to the eclipse part of the orbit (between -50º and 150º longitude). However, even though the wind components are similar at LEO and VLEO, notice that at VLEO the density of the atmosphere is higher. This leads to a higher interaction of the atmosphere molecules with the surfaces of the satellite.

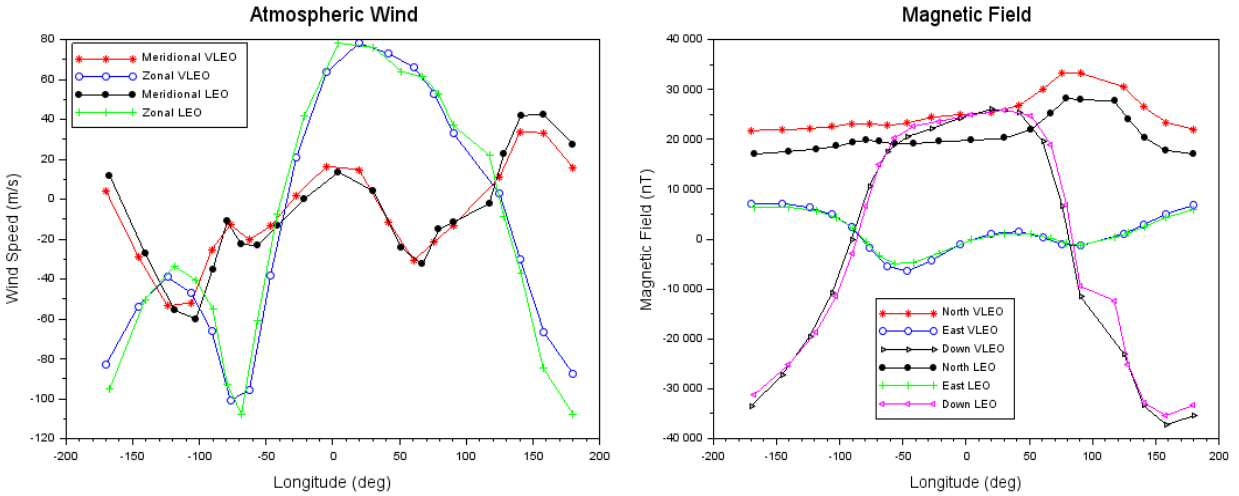

Figure 6: Magnetic field (a) & Horizontal wind (b) components in LEO and VLEO

DOI: 10.13009/EUCASS2019-176

Figure 7 show the attitude control of the 1U satellite carried out with reaction wheels. The initial conditions of the angular velocity were 0.05 *rad/s*, -0.54 *rad/s* and 0.19 *rad/s* for x, y and z components respectively. Notice that in both cases, LEO (7a) and VLEO (7b), the behaviour is similar. This is because the magnitude of the aerodynamic torques is $3.7 \cdot 10^{-9}$ *Nm* for the 1U satellite and the reaction wheels maximum applicable torque is $2.3 \cdot 10^{-3}$ *Nm*, this is three orders of magnitude higher, what means that the reaction wheels easily compensate the torques.

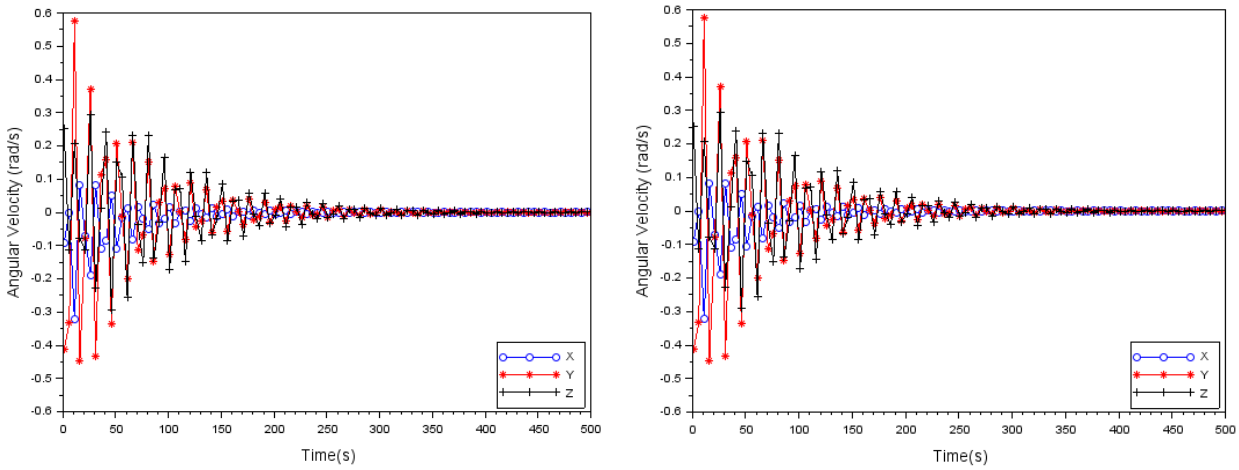

Figure 7: Attitude control of the 1U CubeSat satellite in LEO (700 km) (a) in VLEO (350 km) (b)

Figure 8 and Figure 9 show the apogee and perigee altitude along the lifetime of the 1U satellite for LEO and VLEO respectively. No deorbiting manoeuvres were considered. Besides, the satellite was kept with a constant attitude along the orbit: one of the faces was perpendicular to the tangential direction of the orbit. Notice that the satellite re-enters after 40 years in the LEO scenario and 73 days in the case of the VLEO.

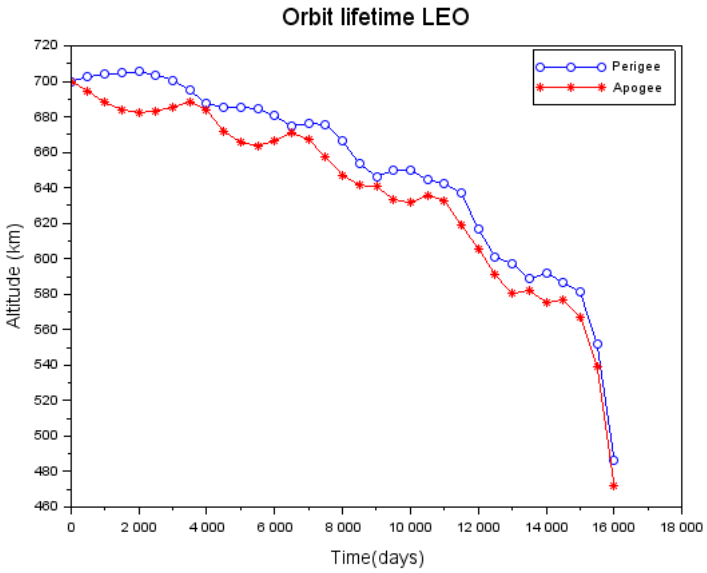

Figure 8: Orbit lifetime for a 1U CubeSat satellite in LEO (700 km)

DOI: 10.13009/EUCASS2019-176

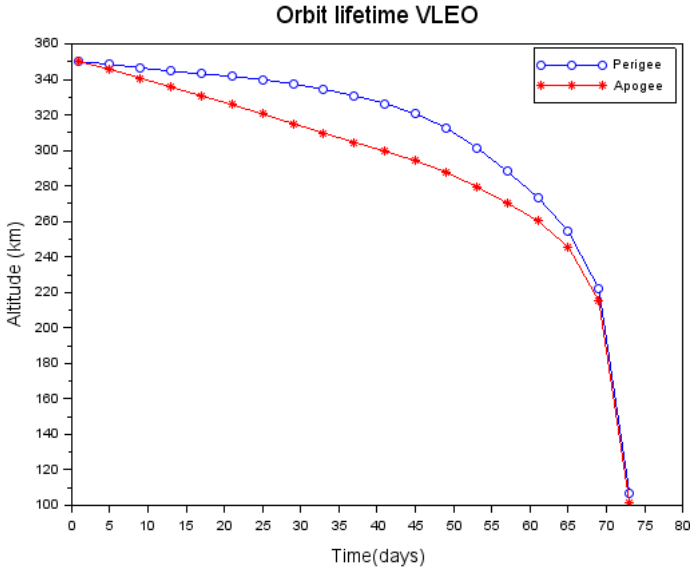

Figure 9: Orbit lifetime for a 1U CubeSat satellite in VLEO (350 km)

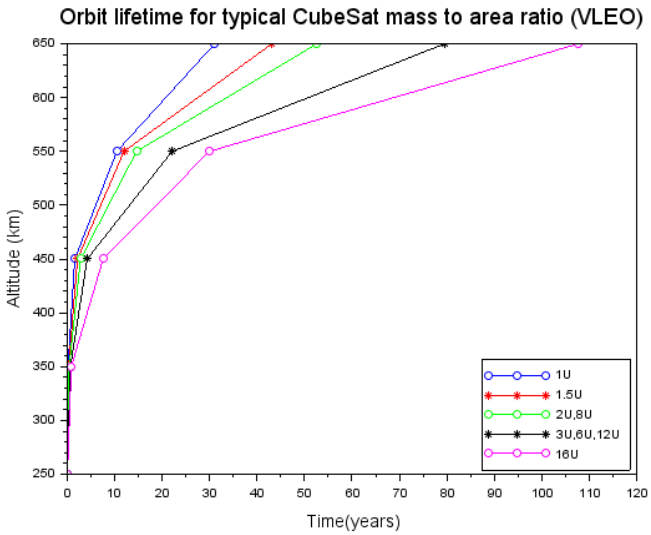

Figure 10: Orbit lifetime in VLEO (350 km) for several types of CubeSats

Figure 10 depicts the time that different CubeSat configurations require to re-enters when flying at different altitudes. To establish the comparison, the mass to area ratio was considered. This is the relation between the frontal area of the satellite and its mass. All the satellites were considered to be flying with constant attitude, in which the frontal face was perpendicular to the tangential direction of the orbit. The 1U CubeSat has a mass to area ratio of 0.01, 2U and 8U have the same mass to area ratio, which is 0.005; 3U, 6U and 12U have the same mass to area ratio, which is $3.33 \cdot 10^{-3}$, and 16U has a mass to area ratio of $2.5 \cdot 10^{-3}$. The picture shows that the 1U satellite is the most unfavourable case because it has the higher mass to area ratio, while the 16U is the most favourable case among all the configurations analyzed.

4. Conclusions

The main implications for a 1U CubeSat flying in VLEO with respect to LEO are at translational level, not rotational, i.e. it highly affects to the altitude of the orbit and its lifetime, more than to the attitude of the satellite. This may change with the configuration and shape of the satellite. The influence at attitude level mainly depends on the shape of the satellite. Therefore, in future works, complex shapes shall be tested to better analyse the effects of VLEO at this level and whether a higher atmospheric density can be used to improve the aptitude behaviour. Finally,

DOI: 10.13009/EUCASS2019-176

the results showed that the mass to area ratio highly affects to the altitude and lifetime of a satellite, indicating that reductions in the mass to area ratio can increase the lifetime of the satellite.

References

[1] Becedas, J., G. González, R.M. Domínguez et al. 2018. Aerodynamic technologies for Earth Observation missions in VLEO. 16th Reinventing Space Conference (RISpace 2018)
[2] Thébault, E., C.C. Finlay, C.D. Beggan, P. Alken et al. 2015. International Geomagnetic Reference Field: the 12th generation. Earth, Planets and Space 67-79. doi:10.1186/s40623-015-0228-9.
[3] S. Bruinsma. 2015. The DTM-2013 thermosphere model. Journal of Space Weather and Space Climate, 5, A1. doi: https://doi.org/10.1051/swsc/2015001.
[4] Drob, D. P., Emmert, J. T., Meriwether, J. W., Makela, J. J., Doornbos, E., Conde, M. & Huba, J. D. 2015. An update to the Horizontal Wind Model (HWM): The quiet time thermosphere. Earth and Space Science, 2(7), 301-319.
[5] Schaaf, S. A. & Chambre, P. A. 1961. Flow of Rarefied Gases. Princeton Aeronautical Paperbacks, Princeton University Press.
[6] R. Schamberg. 1959. A new analytic representation of surface interaction with hypothermal free molecule flow with application to neutral-particle drag estimates of satellites. Technical Report RM-2313, RAND Research Memorandum.
[7] L. H. Sentman. 1961. Free Molecule Flow and its Application to the Determination of Aerodynamic Forces. Lockheed Missiles and Space Co. Inc. Technical report LMSC-448514. Sunnivale. California. Pg.111.
[8] Bird, G. A., & Brady, J. M. 1994. Molecular gas dynamics and the direct simulation of gas flows. Oxford: Clarendon press. Vol. 5.
[9] Moe, K., & Moe, M. M. 2005. Gas–surface interactions and satellite drag coefficients. Planetary and Space Science, 53(8), 793-801. doi:10.1016/j.pss.2005.03.005
[10] M. L. Gargasz. 2007. Optimal Spacecraft Attitude Control Using Aerodynamic Torques. No. AFIT/GA/ENY/07-M08. Air Force Institute of Technology. Ohio.
[11] Pulido, C. L. 2007. Aerodynamic Lift and Drag Effects on the Orbital Lifetime Low Earth Orbit (LEO) Satellites. University of Colorado Boulder.
[12] Walker, A., Mehta, P., & Koller, J. (2014). Drag coefficient model using the cercignani–lampis–lord gas–surface interaction model. Journal of Spacecraft and Rockets, 51(5), 1544-1563.
[13] Mehta, P. M., McLaughlin, C. A., & Sutton, E. K. 2013. Drag coefficient modelling for grace using Direct Simulation Monte Carlo. Advances in Space Research, 52(12), 2035-2051.
[14] Jin, X., Huang, F., & Cheng, X. 2015. Test Particle Monte Carlo Simulation of the Interaction of Two Parallel Flat Plates in Free Molecular Flow Regime. Procedia Engineering, 126, 675–679. doi:10.1016/j.proeng.2015.11.263
[15] Virgili Llop, J., Polat, H. C., & Romano, M. 2019. Attitude Stabilization of Spacecraft in Very Low Earth Orbit by Center-of-Mass Shifting. Frontiers in Robotics and AI, 6, 7.
[16] Traub, C., Romano, F., Binder, T., Boxberger, A., Herdrich, G. H., Fasoulas, S., ... & Crisp, N. H. 2019. On the exploitation of differential aerodynamic lift and drag as a means to control satellite formation flight. CEAS Space Journal, 1-18.